

Carbon-coated lithium titanate: effect of carbon precursor addition processes on the electrochemical performance

Shilei Ding (✉)¹, Zelong Jiang¹, Jing Gu², Hongliang Zhang³, Jiajia Cai¹, Dongdong Wang¹

¹ School of Energy and Environment, Anhui University of Technology, Maanshan 243002, China

² School of Chemistry and Chemical Engineering, Anhui University of Technology, Maanshan 243002, China

³ Analysis and Testing Central Facility, Anhui University of Technology, Maanshan 243002, China

© Higher Education Press 2020

Abstract In this paper, two carbon-coated lithium titanate (LTO-C1 and LTO-C2) composites were synthesized using the ball-milling-assisted calcination method with different carbon precursor addition processes. The physical and electrochemical properties of the as-synthesized negative electrode materials were characterized to investigate the effects of two carbon-coated LTO synthesis processes on the electrochemical performance of LTO. The results show that the LTO-C2 synthesized by using Li_2CO_3 and TiO_2 as the raw materials and sucrose as the carbon source in a one-pot method has less polarization during lithium insertion and extraction, minimal charge transfer impedance value and the best electrochemical performance among all samples. At the current density of $300 \text{ mA} \cdot \text{h} \cdot \text{g}^{-1}$, the LTO-C2 composite delivers a charge capacity of $126.9 \text{ mA} \cdot \text{h} \cdot \text{g}^{-1}$, and the reversible capacity after 300 cycles exceeds $121.3 \text{ mA} \cdot \text{h} \cdot \text{g}^{-1}$ in the voltage range of 1.0–3.0 V. Furthermore, the electrochemical impedance spectra show that LTO-C2 has higher electronic conductivity and lithium diffusion coefficient, which indicates the advantages in electrode kinetics over LTO and LTO-C1. The results clarify the best electrochemical properties of the carbon-coated LTO-C2 composite prepared by the one-pot method.

Keywords lithium titanate, carbon-coated, carbon precursor, synthetic process

1 Introduction

Spinel-type lithium titanate has been considered a promising lithium-ion battery material due to its excellent structural stability and good cycle life, especially suitable

for large-scale energy storage [1–3]. Lithium titanate (LTO), which is called “zero strain material”, has zero volume change during the lithium insertion/extraction and shows an excellent cycling property [4,5]. Moreover, LTO has outstanding safety characteristics with a high lithium intercalation potential (1.55 V vs. Li^0/Li^+) during discharge, which can also avoid the formation of lithium dendrites and solid electrolyte interphase [1,4]. However, the low electronic conductivity ($< 10^{-13} \text{ S} \cdot \text{cm}^{-1}$) and lithium diffusion coefficient of LTO materials severely limits their high rate capability [5].

To improve the electrochemical performance of LTO, one method is to fabricate nano LTO materials with different morphologies [6–9], shorten the diffusion path of lithium in the solid-state, and enhance the intercalation kinetics. The other method is to modify LTO materials using a doping [10–12] or conducting agent [13–16] to improve the electronic conductivity and Li ion diffusion efficiency. Among them, there are various methods to fabricate LTO composites by using carbon as a conductive agent, e.g., amorphous carbon [17–19], porous carbon [20], carbon nanotube [21–24] and graphene [25–27]. Tang [28] fabricated graphene-supported LTO nanosheets by using graphene oxide sheets as a precursor in a hydrothermal reaction, and Sun [29] prepared mesoporous LTO nanoclusters in carbon nanotubes using a solution method. The LTO composites showed high performance. The sol-gel method was used to coat the carbon-modified LTO with carbon again, which reduced the particle size, promoted the formation of trivalent titanium, and increased the high rate and cycle life. Flexible $\text{Li}_4\text{Ti}_5\text{O}_{12}$ carbon nanofibers are made on nonwoven fabrics by electrospinning [30]. LTO particles (~50 nm) on this flexible composite film are closely connected to the 3D flexible nonwoven fabric film, which exhibits high speed and reversible cycling performance. Hierarchical ultrathin LTO nanosheets were *in situ* synthesized inside the carbon

nanotubes via a precursor morphology-controlled conversion strategy, which has more stable cycling and better rate capacity [23].

All of the above synthesis methods can improve the electrochemical performance of LTO, but expensive precursors or relatively complex synthesis are required to achieve better materials, and the manufacturing cost of the materials is increased. The solid-phase calcination method with a wide range of raw materials, low cost, and simple process is worthy of study, although there are problems such as the choice of carbon precursor, process sequence, and degree of combination of carbon and LTO, which affects the battery performance. Here, carbon-coated LTO was prepared by solid-phase calcination, and the effect of carbon precursor synthetic processes on the electrochemical performance of the carbon-coated LTO electrode material was explored to optimize the modification route.

2 Experimental

2.1 Material preparation and characterizations

Preparation of the LTO. All starting reagents were of analytical grade, and the deionized water was used throughout the study. Firstly, 1.22 g Li_2CO_3 , 3.20 g TiO_2 powders and 4.40 mL of deionized water were mixed, then the slurry mixture was placed in an agate tank for planetary ball milling for 5 h ($300 \text{ r} \cdot \text{min}^{-1}$). The ground white slurry was dried in a vacuum oven at $80 \text{ }^\circ\text{C}$ for 1 h and calcined in a tubular resistance furnace at $800 \text{ }^\circ\text{C}$ for 12 h under N_2 atmosphere to obtain pure LTO.

Preparation of the carbon-coated LTO-C1 and LTO-C2. As shown in Fig. 1, two different carbon-coating processes were used to modify LTO. (a) Two-step preparation of LTO-C1. First, 0.41 g sucrose was put into a crucible and sintered at $800 \text{ }^\circ\text{C}$ for 6 h in a tube furnace filled with nitrogen at a heating rate of $10 \text{ }^\circ\text{C} \cdot \text{min}^{-1}$ to obtain a carbon material. Then, the carbon and prepared LTO were mixed and ball-milled for 5 h, and the subsequent treatment process is identical to the LTO process. (b) Synthesis of

LTO-C2 by one-pot ball-assisted calcination. Initially, 1.22 g Li_2CO_3 , 3.20 g TiO_2 and 0.41 g sucrose were mixed and placed in a planetary ball mill. The subsequent processing was identical to the preparation of the sample LTO.

The crystal structures of the obtained samples were analyzed by X-ray diffraction (XRD, Bruker D8) with $\text{Cu K}\alpha$ radiation ($10^\circ < 2\theta < 90^\circ$). The morphologies and structures of the obtained composites were characterized by Field Emission Scanning Electron Microscopy (FE-SEM, NANO SEM430) and High Resolution Transmission Electron Microscopy (HRTEM, JEM-2100, 200 KV). Raman spectra were recorded on a Renishaw inVia confocal Raman spectroscope (Renishaw, Gloucestershire, UK) equipped with a 532-nm laser. Thermogravimetric analysis (TGA) was performed by using a DTG-60H instrument (Shimadzu Co.). Heating ramps from room temperature to $900 \text{ }^\circ\text{C}$ at $10 \text{ }^\circ\text{C} \cdot \text{min}^{-1}$ were performed in air with a gas flow of $50 \text{ mL} \cdot \text{min}^{-1}$.

2.2 Coin cell assembly

Electrode preparation. The prepared active material, acetylene black and polyvinylidene fluoride (PVDF) (6:3:1 mass ratio) were mixed to form a paste and evenly coated on a copper foil in a vacuum drying oven at $105 \text{ }^\circ\text{C}$ for 12 h.

Battery assembly. Li metal foil, Cegard 2300 polypropylene porous membrane, $1 \text{ mol} \cdot \text{L}^{-1}$ LiPF_6 in dimethyl carbonate: ethylene carbonate with a volume ratio of 1:1 were used as the counter electrode, separator and electrolyte, respectively. The CR2025 button batteries were assembled in an argon-filled glove box with the as-obtained film and left for 12 h.

2.3 Electrochemical measurements

The charge/discharge performance of the samples were detected by using Galvanostatic testing (CT2001A Land Battery Test System, Wuhan Lanhe, China) between 1.0 V and 3.0 V at different rates.

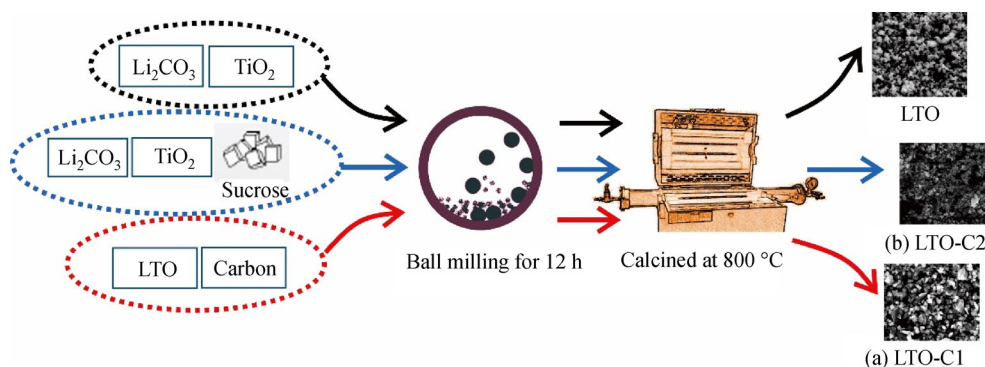


Fig. 1 Synthesis procedure of the LTO, LTO-C1 and LTO-C2 composites.

Cyclic voltammograms (CV) were performed in the range of 1.0–3.0 V (vs. Li/Li⁺) with a scan rate of 0.1 mV·s⁻¹ using a CHI 1000C electrochemical workstation. The experimental temperature was 25 °C ± 0.5 °C. Electrochemical impedance spectroscopy (EIS) tests were performed using PARSTAT 4000 electrochemical workstation with a frequency range of 10⁴–0.01 Hz.

3 Results and discussion

The XRD patterns of the LTO, LTO-C1 and LTO-C2 composite are shown in Fig. 2. For pure LTO, the major diffraction peaks can be indexed to (111), (311), (400), (331), (333), (440), (531) and (533) of cubic spinel LTO (JCPDS#49-0207), and the diffraction peaks are sharp, which indicates that the prepared LTO has good crystallinity. For the carbon-coated LTO-C1 and LTO-C2 prepared by different synthetic processes, the diffraction patterns of LTO remain, and no other impurity peaks were found. The carbon coating did not affect the formation of cubic spinel LTO.

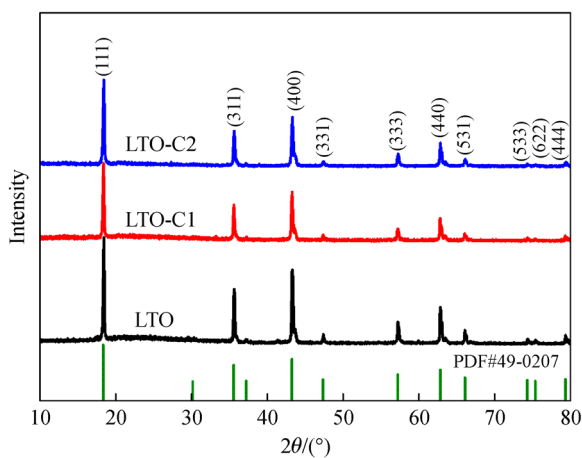


Fig. 2 XRD patterns of LTO, LTO-C1 and LTO-C2 samples.

The D and G Raman peaks are ascribed to the disorder of carbon and the vibrations of graphitic sp² carbon, respectively. The intensity ratio of D and G (I_D/I_G) reflects the disorder degree in the materials [16]. In Fig. 3, the D and G bands are clearly observed for LTO-C1 and LTO-C2, which indicates the graphitization of the carbon component. Moreover, the I_D/I_G ratio of LTO-C2 (0.83) is higher than that of LTO-C1 (0.60), which suggests that a higher degree of disorder in LTO-C2 may favor its better electrochemical properties.

To calculate the carbon content of the carbon-coated materials, thermal characterization of the materials was performed using TGA in air. Figure 4 shows the TGA curves of the LTO-C1 and LTO-C2 samples. LTO-C1 and LTO-C2 show obvious and similar weight losses. The

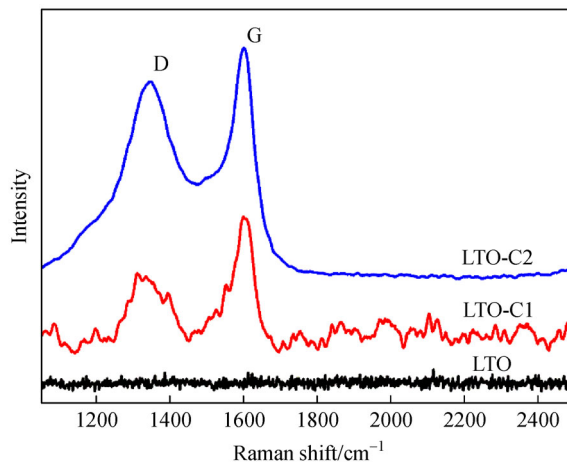


Fig. 3 Raman spectra of LTO, LTO-C1 and LTO-C2 samples with 514 nm excitation of an argon ion laser.

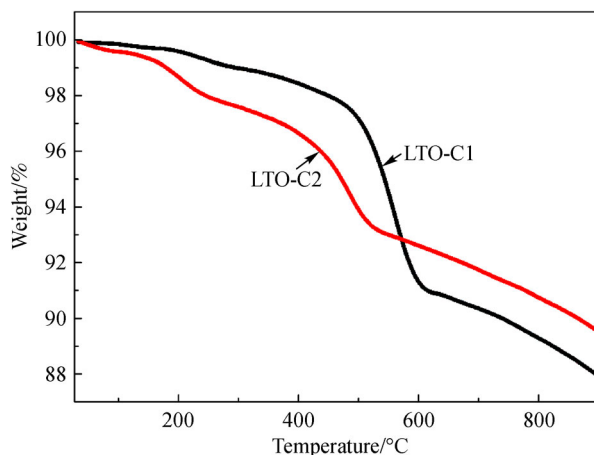


Fig. 4 Thermal analysis curves of LTO-C1 and LTO-C2 samples in air atmosphere.

weight loss before 350 °C comes from the evaporation and dehydration of adsorbed and surface water from the samples. In addition, the weight loss in the temperature range of 350 °C–700 °C is caused by the reaction of carbon in the sample with oxygen in the air [31]. However, compared with LTO-C1, the carbon loss in LTO-C2 moves to a lower temperature zone. The difference may be due to the processing methods. The SEM and HRTEM characterization (Figs. 5 and 6) show that the carbon distribution in the LTO-C2 sample is uniform and thin. The structural feature of LTO-C2 is conducive to the full combustion of carbon. From the weight loss, the carbon contents in the LTO-C1 and LTO-C2 samples were 7.9% and 5.6%, respectively.

The differences in morphology and structure of LTO, LTO-C1 and LTO-C2 can be confirmed by SEM and HRTEM images. Figure 5 shows the SEM images of the

samples prepared by two different processing processes. Pure LTO has submicron particles with a relatively uniform distribution, and its particle size is 200–600 nm as shown in Fig. 5(a). The LTO-C1 sample is shown in Fig. 5(b). Lumpy carbon particles of various sizes are mixed in the middle of pure LTO particles. Thus, the amorphous carbon is physically intertwined with LTO particles in the two-step preparation method, and the carbon material cannot be sufficiently coated on the lithium titanium oxide material.

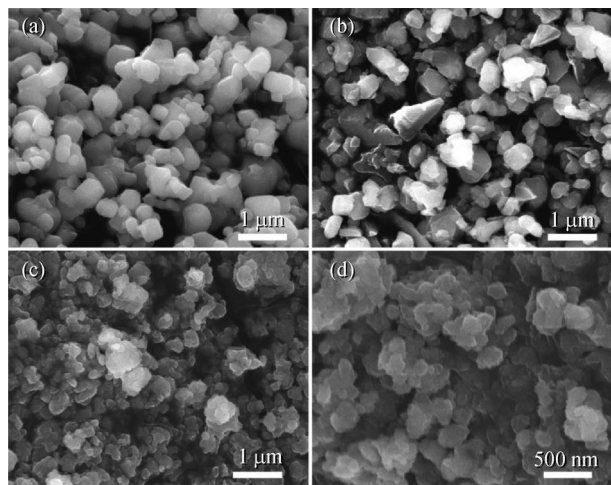


Fig. 5 SEM images of (a) LTO, (b) LTO-C1, and (c, d) LTO-C2 samples.

Unlike the obvious isolation between carbon and LTO in LTO-C1, in Figs. 5 (c, d), especially the parts marked with dashed lines, carbon and LTO are closely connected to form a good composite, which is beneficial to the electrolyte penetration and lithium migration. The particle size of LTO-C2 is mainly distributed between 50 nm and 200 nm, which is smaller than the particle size of LTO-C1. The carbon precursor and LTO precursor are fully mixed to reduce the LTO agglomeration effect. Thus, carbon coating using the one-pot method can inhibit the growth and agglomeration of LTO particles.

To further examine the grain size and crystal structure of the as-synthesized samples, the pure LTO, LTO-C1 and LTO-C2 composites were also investigated by HRTEM as shown in Fig. 6. The grain size of LTO particles is 200 or 600 nm. In Fig. 6(b), a clear crystal lattice can be found with a layer spacing of 0.48 nm, which corresponds to the (111) crystal faces of LTO. The results are consistent with the XRD results in Fig. 2. LTO-C1 (Figs. 6(c, d)) shows the relatively independent coexistence of carbon particles and LTO particles, which is consistent with the SEM results in Fig. 5(b). In Fig. 6(f), the amorphous nanocarbon of LTO-C2 was coated on the surface of LTO particles during the heat treatment process. After the high-energy ball milling, sucrose was thoroughly mixed in the LTO precursors and

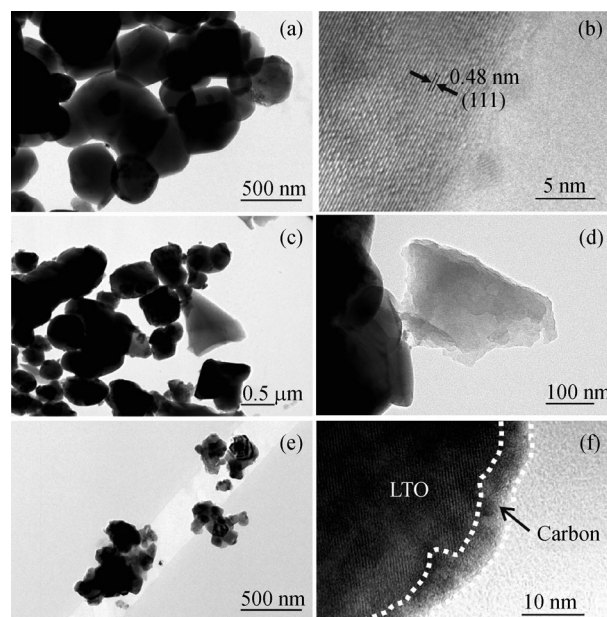


Fig. 6 HRTEM images of (a, b) LTO, (c, d) LTO-C1 and (e, f) LTO-C2 composites.

calcined to pyrolyze into conductive carbon. The above comparative analysis shows that simple mechanical mixing cannot obtain a uniform carbon coating material, but through the one-pot synthesis, carbon can inhibit the growth of LTO particles and promote the generation of uniformly dispersed nanostructures, which expands the electronic pathway and will be beneficial to unblocked electronics.

Figures 7(a, b) display the rate performance curves of pure LTO, LTO-C1 and LTO-C2 at different charge/discharge rates. When the current density increases, the charge/discharge specific capacity of all materials are attenuated to varying degrees, which may be related to the capacity degradation due to the irreversible extraction of lithium ions under high current.

The first discharge specific capacities of the materials at a current density of $50 \text{ mA} \cdot \text{g}^{-1}$ were 124.6, 137.4 and $142.3 \text{ mA} \cdot \text{g}^{-1}$. With the increase in current density, carbon-coated LTO has higher specific discharge capacity than pure LTO, which shows that the carbon addition makes it easier for Li^+ to insert and extract Li, while pure LTO particles agglomerate to form large particles and cause severe polarization and faster specific capacity decay. Moreover, carbon and LTO are tighter and more uniform in LTO-C2 than in LTO-C1, which can effectively improve the electrical conductivity of electrons in the LTO-C2 composite.

Figure 8 shows the cycle performance of LTO-C at a current density of $300 \text{ mA} \cdot \text{g}^{-1}$. The electrochemical performances of the samples are relatively stable without much fluctuation in single rate conditions. LTO-C2 has higher charge-discharge specific capacitance than

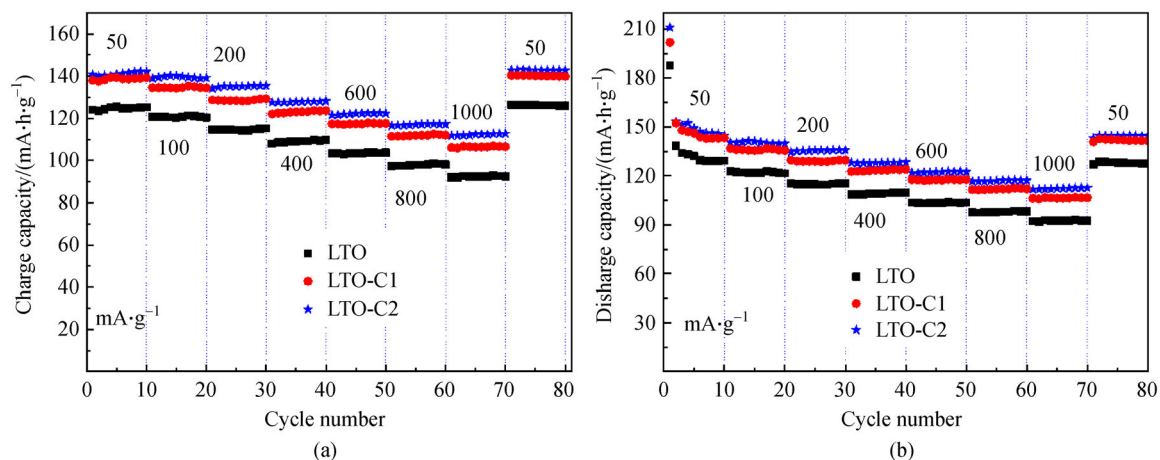


Fig. 7 Rate performance of (a) charge and (b) discharge at different rates of LTO, LTO-C1 and LTO-C2.

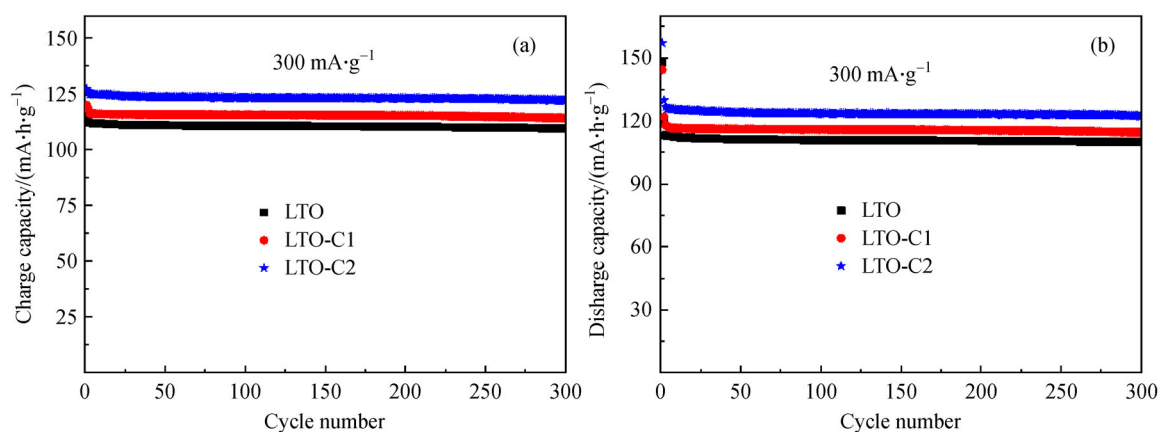


Fig. 8 Cycle performance of the (a) charge and (b) discharge of LTO, LTO-C1 and LTO-C2.

LTO and LTO-C1, the first charge specific capacity is $126.9 \text{ mA} \cdot \text{h} \cdot \text{g}^{-1}$, and the irreversible capacity loss is only 4.2% after 300 cycles. However, LTO-C1 has a limited increase in Li^+ diffusion capacity due to the loose relationship between carbon and LTO. Therefore, LTO-C2 is more conducive to improve the electrochemical performance.

The initial coulombic efficiencies of LTO, LTO-C1 and LTO-C2 at different rates of charge and discharge are 79.5%, 81.3% and 82.9%, respectively. The results are shown in the inset of Fig. 9. After 10 cycles, the coulombic efficiency of pure LTO and carbon-coated LTO composites is close to 100%, which is an acceptable initial coulombic efficiency.

The curves in Fig. 10 show that each sample has a pair of redox peaks in the range of 1.4–1.8 V, which corresponds to the valence state conversion between Ti^{4+} and Ti^{3+} . The electrochemical process of the electrode is the insertion and extraction of Li^+ in LTO. The difference of redox peaks is related to the migration of lithium ions. The difference values of LTO-C2 are the smallest of the three

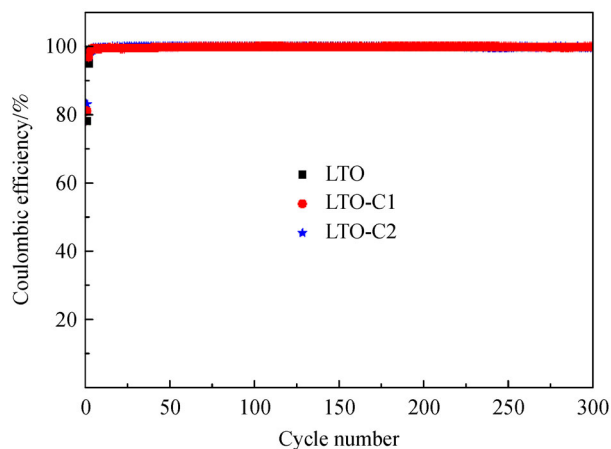


Fig. 9 Coulombic efficiencies of LTO, LTO-C1 and LTO-C2.

negative electrodes, which indicates the small polarization and best reversibility.

To further study the lithiation kinetics of pure LTO,

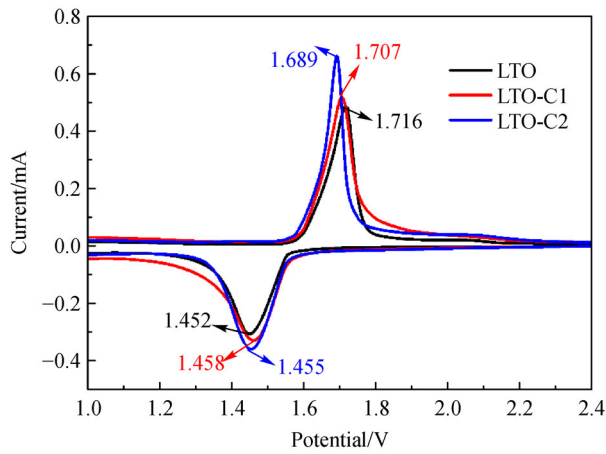


Fig. 10 Cyclic voltammograms of LTO, LTO-C1 and LTO-C2.

LTO-C1 and LTO-C2 composites, Nyquist plots of the electrodes before cycles are displayed in Fig. 11. All plots are composed of two parts: a semicircle is related to the charge transfer resistance in the high-frequency region, and a slope line in the low-frequency region corresponds to the diffusion of lithium ions into the electrode material lattice.

The inserted graph in Fig. 11(a) shows the equivalent circuit, where the charge transfer resistance, solution ohmic resistance, double layer capacitance and Warburg impedance are represented by R_{ct} , R_s , constant phase element and Z_w [32]. The fitted results (inset table in Fig. 11(a)) clearly show that the LTO-C1 and LTO-C2 electrodes have smaller R_{ct} (278.9 and 230.7 Ω , respectively) than pure LTO (534.5 Ω). Thus, adding carbon to LTO facilitates the lithium ion conduction. The two processes of carbon addition result in different results. LTO-C2 has better electrochemical kinetics than LTO-C1.

Furthermore, the Li^+ diffusion coefficient (D_{Li^+}) can be calculated as follows [23,33]:

$$D_{\text{Li}} = \frac{R^2 T^2}{2A^2 n^4 F^4 C_{\text{Li}}^2 \sigma^2}, \quad (1)$$

$$Z_{\text{re}} = R_{\text{ct}} + R_s + \sigma \omega^{-0.5}, \quad (2)$$

where n is the number of electrons per molecule during oxidation, R is the gas constant, A is the surface area of the electrode, T is the absolute temperature, F is Faraday constant, C_{Li} is the concentration of lithium ions, and ω is the angular frequency. As shown in Fig. 11(b), the slope of the Z_{re} vs. $\omega^{-0.5}$ curve of LTO-C2 is higher than those of pure LTO and LTO-C1, which indicates that LTO-C2 exhibits a higher Li^+ transfer coefficient. The Li^+ diffusion coefficients of LTO, LTO-C1 and LTO-C2 are 4.9×10^{-16} , 1.14×10^{-15} and 1.0×10^{-14} $\text{cm}^2 \cdot \text{s}^{-1}$, respectively. LTO-C2 has the higher lithium diffusion coefficient than LTO and LTO-C1. The results reveal that the carbon coating by one-pot synthesis method can improve the lithium diffusion coefficient of LTO-C2, which exhibits a higher rate performance than pure LTO and LTO-C1 at high rates.

4 Conclusions

In summary, two different synthesis methods were used to prepare carbon-coated LTO electrode materials, which verified the effects of different carbon treatment processes on the electrochemical performance of carbon-coated LTO. The results show that the carbon coating material has better performance than pure LTO. As a conductive matrix, carbon can quickly provide electrons for LTO to help its storage. More importantly, the material prepared by the one-pot method performs better than the carbon-coated LTO prepared by the two-step method. In one-pot synthesis, carbon precursors provide support to anchor well-dispersed LTO, which can inhibit the accumulation and growth of LTO nanoparticles during the calcination

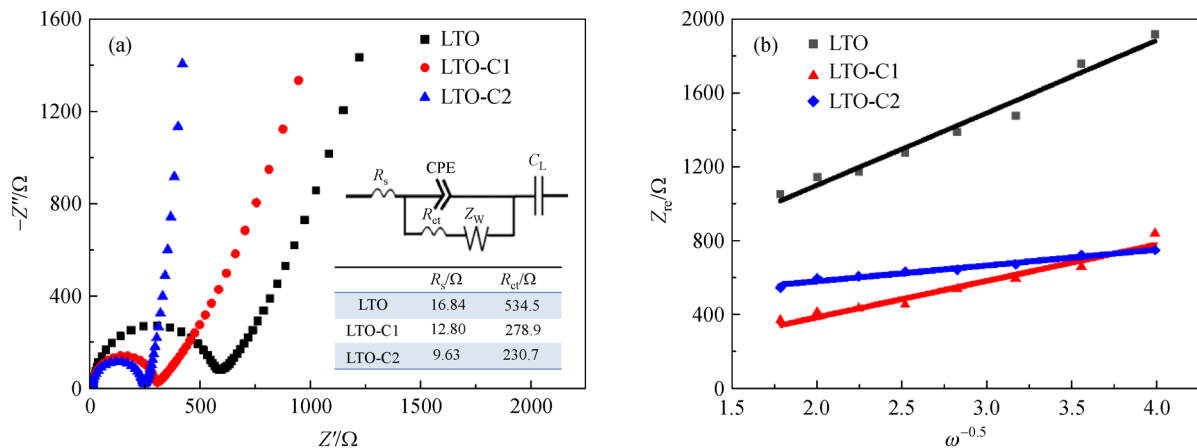


Fig. 11 (a) EIS patterns of LTO, LTO-C1 and LTO-C2; (b) Corresponding linear fitting of Warburg impedance.

process and reduce the length of lithium ion and electron transport paths. Mutually, LTO is dispersed in the carbon precursor, which reduces the high degree of polymerization of carbon and maintains a large active contact area between the electrode and the electrolyte. Therefore, the carbon-coated LTO prepared by the one-pot method shows better rate performance and stability. In addition, the method can easily obtain raw materials at a low cost and has a simple process, which is a good strategy for developing high-performance spinel LTO materials.

References

1. Yue J P, Badaczewski F M, Voepel P, Leichtweiß T, Mollenhauer D, Zeier W G, Smarsly B M. Critical role of the crystallite size in nanostructured $\text{Li}_4\text{Ti}_5\text{O}_{12}$ anodes for lithium-ion batteries. *ACS Applied Materials & Interfaces*, 2018, 10(26): 22580–22590
2. Yi T F, Yang S Y, Xie Y. Recent advances of $\text{Li}_4\text{Ti}_5\text{O}_{12}$ as a promising next generation anode material for high power lithium-ion batteries. *Journal of Materials Chemistry. A, Materials for Energy and Sustainability*, 2015, 3(11): 5750–5777
3. Zhang T, Paillard E. Recent advances toward high voltage, EC-free electrolytes for graphite-based Li-ion battery. *Frontiers of Chemical Science and Engineering*, 2018, 12(3): 577–591
4. Cao S M, Feng X, Song Y Y, Liu H J, Miao M, Fang J H, Shi L Y. *In situ* carbonized cellulose-based hybrid film as flexible paper anode for lithium-ion batteries. *ACS Applied Materials & Interfaces*, 2016, 8(2): 1073–1079
5. Cheng J, Che R C, Liang C Y, Liu J W, Wang M, Xu J J. Hierarchical hollow $\text{Li}_4\text{Ti}_5\text{O}_{12}$ urchin-like microspheres with ultra-high specific surface area for high rate lithium ion batteries. *Nano Research*, 2014, 7(7): 1043–1053
6. Ge H, Hao T T, Osgood H, Zhang B, Chen L, Cui L X, Song X M, Ogoke O, Wu G. Advanced mesoporous spinel $\text{Li}_4\text{Ti}_5\text{O}_{12}$ /RGO composites with increased surface lithium storage capability for high-power lithium-ion batteries. *ACS Applied Materials & Interfaces*, 2016, 8(14): 9162–9169
7. Feng X Y, Zou H L, Xiang H F, Guo X, Zhou T P, Wu Y C, Xu W, Yan P F, Wang C M, Zhang J G, Yu Y. Ultrathin $\text{Li}_4\text{Ti}_5\text{O}_{12}$ nanosheets as anode materials for lithium and sodium storage. *ACS Applied Materials & Interfaces*, 2016, 8(26): 16718–16726
8. Han M C, Zhang J H, Li Y M, Zhu Y R, Yi T F. $\text{Li}_5\text{Cr}_7\text{Ti}_6\text{O}_{25}$ /multiwalled carbon nanotubes composites with fast charge-discharge performance as negative electrode materials for lithium-ion batteries. *Journal of the Electrochemical Society*, 2019, 166(4): A626–A634
9. Haridas A K, Sharma C S, Rao T N. Donut-shaped $\text{Li}_4\text{Ti}_5\text{O}_{12}$ structures as a high performance anode material for lithium ion batteries. *Small*, 2015, 11(3): 290–294
10. Zou S, Wang G, Zhang Y M, Xue C H, Chen H Y, Yang G J, Nan H, Wei H M, Lin H. Nano-structure and characterization of carbon composite with Al^{3+} and Mn^{4+} co-doped $\text{Li}_4\text{Ti}_5\text{O}_{12}$ as anodes for Li-ion batteries. *Journal of Alloys and Compounds*, 2020, 816: 152609
11. Wang Z Y, Sun L M, Yang W Y, Yang J B, Sun K, Chen D F, Liu X F. Unveiling the synergic roles of Mg/Zr co-doping on rate capability and cycling stability of $\text{Li}_4\text{Ti}_5\text{O}_{12}$. *Journal of the Electrochemical Society*, 2019, 166(4): A658–A666
12. Zhang H Q, Deng Q J, Mou C X, Huang Z L, Wang Y, Zhou A J, Li J Z. Surface structure and high-rate performance of spinel $\text{Li}_4\text{Ti}_5\text{O}_{12}$ coated with N-doped carbon as anode material for lithium-ion batteries. *Journal of Power Sources*, 2013, 239: 538–545
13. Zeng Q, Wu J N, Yu Z H, Luo L G. Conductive PEDOT-decorated $\text{Li}_4\text{Ti}_5\text{O}_{12}$ as next-generation anode material for electrochemical lithium storage. *Solid State Ionics*, 2018, 325: 7–11
14. Stenina I A, Shaydullin R R, Kulova T L, Skundin A M, Yaroslavtsev A B. Influence of carbon coating and PANI modification on the electrochemical performance of $\text{Li}_4\text{Ti}_5\text{O}_{12}$. *Ionics*, 2019, 25(5): 2077–2085
15. Wang Y X, Tian W, Wang L H, Zhang H R, Liu J L, Peng T Y, Pan L, Wang X B, Wu M B. A tunable molten-salt route for scalable synthesis of ultrathin amorphous carbon nanosheets as high-performance anode materials for lithium-ion batteries. *ACS Applied Materials & Interfaces*, 2018, 10(6): 5577–5585
16. Li B H, Han C P, He Y B, Yang C, Du H D, Yang Q H, Kang F Y. Facile synthesis of $\text{Li}_4\text{Ti}_5\text{O}_{12}$ /C composite with super rate performance. *Energy & Environmental Science*, 2012, 5(11): 9595–9602
17. Zheng L Y, Wang X Y, Xia Y G, Xia S L, Metwalli E, Qiu B, Ji Q, Yin S S, Xie S, Fang K, et al. Scalable *in situ* synthesis of $\text{Li}_4\text{Ti}_5\text{O}_{12}$ /carbon nanohybrid with supersmall $\text{Li}_4\text{Ti}_5\text{O}_{12}$ nanoparticles homogeneously embedded in carbon matrix. *ACS Applied Materials & Interfaces*, 2018, 10(3): 2591–2602
18. Lu H R, Hagberg J, Lindbergh G, Cornell A. $\text{Li}_4\text{Ti}_5\text{O}_{12}$ flexible, lightweight electrodes based on cellulose nanofibrils as binder and carbon fibers as current collectors for Li-ion batteries. *Nano Energy*, 2017, 39: 140–150
19. Yao N Y, Liu H K, Liang X, Sun Y, Feng X Y, Chen C H, Xiang H F. $\text{Li}_4\text{Ti}_5\text{O}_{12}$ nanosheets embedded in three-dimensional amorphous carbon for superior-rate battery applications. *Journal of Alloys and Compounds*, 2019, 771: 755–761
20. Rath P C, Mishra M, Saikia D, Chang J K, Perng T P, Kao H M. Facile fabrication of titania-ordered cubic mesoporous carbon composite: effect of Ni doping on photocatalytic hydrogen generation. *International Journal of Hydrogen Energy*, 2019, 44(35): 19255–19266
21. Zhao S, Zhang M M, Wang Z H, Xian X C. Enhanced high-rate performance of $\text{Li}_4\text{Ti}_5\text{O}_{12}$ microspheres/multiwalled carbon nanotubes composites prepared by electrostatic self-assembly. *Electrochimica Acta*, 2018, 276: 73–80
22. Tang Y K, Liu L, Zhao H Y, Kong L B, Guo Z P, Gao S S, Che Y Y, Wang L, Jia D Z. Rational design of hybrid porous nanotubes with robust structure of ultrafine $\text{Li}_4\text{Ti}_5\text{O}_{12}$ nanoparticles embedded in bamboo-like cnts for superior lithium ion storage. *Journal of Materials Chemistry. A, Materials for Energy and Sustainability*, 2018, 6(8): 3342–3349
23. Jiao W L, Chen C, Liang C Y, Che R C. Preparation of carbon nanotube coated $\text{Li}_4\text{Ti}_5\text{O}_{12}$ nanosheets heterostructure as ultrastable anodes for lithium-ion batteries. *ACS Applied Energy Materials*, 2018, 1(11): 6352–6360
24. Tang Y K, Liu L, Zhao H Y, Jia D Z, Liu W. Porous CNT@

- $\text{Li}_4\text{Ti}_5\text{O}_{12}$ coaxial nanocables as ultra high power and long life anode materials for lithium ion batteries. *Journal of Materials Chemistry. A, Materials for Energy and Sustainability*, 2016, 4(6): 2089–2095
25. Zhu K X, Gao H Y, Hu G X. A flexible mesoporous $\text{Li}_4\text{Ti}_5\text{O}_{12}$ -RGO nanocomposite film as free-standing anode for high rate lithium ion batteries. *Journal of Power Sources*, 2018, 375: 59–67
26. Li S J, Mao J. The influence of different types of graphene on the lithium titanate anode materials of a lithium ion battery. *Journal of Electronic Materials*, 2018, 47(9): 5410–5416
27. Qian Y, Cai X Y, Zhang C Y, Jiang H F, Zhou L J, Li B S, Lai L F. A free-standing $\text{Li}_4\text{Ti}_5\text{O}_{12}$ /graphene foam composite as anode material for Li-ion hybrid supercapacitor. *Electrochimica Acta*, 2017, 258: 1311–1319
28. Tang Y F, Huang F Q, Zhao W, Liu Z Q, Wan D Y. Synthesis of graphene-supported $\text{Li}_4\text{Ti}_5\text{O}_{12}$ nanosheets for high rate battery application. *Journal of Materials Chemistry*, 2012, 22(22): 11257–11260
29. Sun L, Kong W B, Wu H C, Wu Y, Wang D T, Zhao F, Jiang K L, Li Q Q, Wang J P, Fan S S. Mesoporous $\text{Li}_4\text{Ti}_5\text{O}_{12}$ nanoclusters anchored on super-aligned carbon nanotubes as high performance electrodes for lithium ion batteries. *Nanoscale*, 2016, 8(1): 617–625
30. Zhang Z B, Deng X, Sunarso J K, Cai R, Chu S Y, Miao J, Zhou W, Shao Z P. Two-step fabrication of $\text{Li}_4\text{Ti}_5\text{O}_{12}$ -coated carbon nanofibers as a flexible film electrode for high-power lithium-ion batteries. *ChemElectroChem*, 2017, 4(9): 2286–2292
31. Li Z T, Wang Y K, Sun H D, Wu W T, Liu M, Zhou J Y, Wu G L, Wu M B. Synthesis of nanocomposites with carbon-SnO₂ dual-shells on TiO₂ nanotubes and their application in lithium ion batteries. *Journal of Materials Chemistry. A, Materials for Energy and Sustainability*, 2015, 3(31): 16057–16063
32. Li X, Huang P X, Zhou Y, Peng H, Li W, Qu M Z, Yu Z L. A novel $\text{Li}_4\text{Ti}_5\text{O}_{12}$ /graphene/carbon nano-tubes hybrid material for high rate lithium ion batteries. *Materials Letters*, 2014, 133: 289–292
33. Chou S L, Wang J Z, Liu H K, Dou S X. Rapid synthesis of $\text{Li}_4\text{Ti}_5\text{O}_{12}$ microspheres as anode materials and its binder effect for lithium-ion battery. *Journal of Physical Chemistry C*, 2011, 115(32): 16220–16227